Journal of Materials Chemistry

Cite this: J. Mater. Chem., 2012, 22, 16399

www.rsc.org/materials

PAPER

Graphite oxide, graphene, and metal-loaded graphene for fire safety applications of polystyrene

Chenlu Bao,[a] Lei Song,[a] Charles A. Wilkie,[b] Bihe Yuan,[a] Yuqiang Guo,[a] Yuan Hu*[a] and Xinglong Gong*[ac]

Received 20th April 2012, Accepted 11th June 2012
DOI: 10.1039/c2jm32500d

Graphite oxide, graphene, ZrO_2-loaded graphene and β-$Ni(OH)_2$-loaded graphene (joint appellation: Gs) were prepared and incorporated into polystyrene so as to improve the fire safety properties of polystyrene. By the masterbatch-melt blending technique, Gs nanolayers were well dispersed and exfoliated in polystyrene as thin layers (thickness 0.7–2 nm). The fire safety properties were visibly improved, including an increased thermal degradation temperature (18 °C, PS/Ni–Gr-2), decreased peak heat release rate (40%, PS/Zr–Gr-2) and reduced CO concentration (54%, PS/Ni–Gr-2). The mechanism for the improved thermal stability and fire safety properties was investigated based on this study and previous works. The physical barrier effect of graphene, the interaction between graphene and polystyrene, and the synergistic effect of the metal compounds are the causes for the improvements.

1. Introduction

Graphene, a carbon monolayer with unique properties such as quantum effects, dramatic strength, high electron mobility, thermal conductivity and stability, has gained much interest over the last few years. Graphene is promising in many applications, including energy storage materials, sensors, conducting materials and high-performance composites, *etc.*[1–4] The future of graphene is bright, however, the road to the realistic application of graphene is long and winding since graphene science is still young.[5]

Very recently, we reported a new application of graphene to enhance the fire safety of polymer-based composites.[6–8] Polymers usually are easily ignited and burned. In recent years, polymer-based foam has caused several serious fires in China, so the fire safety properties of polymers have attracted a lot of attention.[9,10] The heat, smoke and toxic gases released in fires are the main causes of injury and death. Compared with virgin polymers, the amount of heat and toxic gas released are decreased in graphene/polymer nanocomposites (GPNCs) when they were burned.[6,7] For example, the peak heat release rate (PHRR) of graphene/poly(lactic acid) (PLA) nanocomposites was reduced by 40%.[6] However, as a truly new application of graphene, there are still many problems to be solved: (1) the fire safety properties of GPNCs should be visibly improved; (2) the mechanism of the improvements should be clarified; and (3) the preparation of GPNCs must be feasible for the use of industrial processing techniques.

Nanocomposites consisting of a polymer matrix and layered nanofillers, such as clays and double hydroxides, are widely used to improve the fire safety properties of polymers.[11–14] Transition metal elements such as nickel, iron and zirconium are efficient at improving fire safety properties.[15–17] Therefore, the combination of the nanocomposite technique and metal compounds may pioneer a new and efficient method to achieve good fire safety properties in polymers. Herein, graphite oxide (GO), graphene, ZrO_2-loaded graphene (Zr–Gr) and β-$Ni(OH)_2$-loaded graphene (Ni–Gr) (joint appellation: Gs) were prepared and incorporated into polystyrene (PS) for fire safety applications. Zr–Gr and Ni–Gr were prepared by the hydrothermal method (Fig. 1). PS is a popular polymer with wide ranging applications such as foams, thermal insulation materials, architectural materials and furniture,[18,19] which has caused several serious fires recently.[10]

Various improvements have been obtained with graphene/PS composites, such as electrical conductivity, mechanical properties and thermal stability, but there is little work on fire safety.[20–24] The improved thermal stability, which is an important

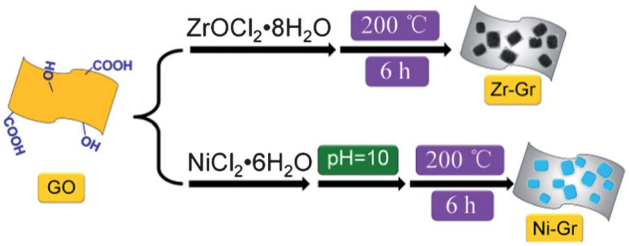

Fig. 1 Hydrothermal synthesis of Zr–Gr and Ni–Gr.

[a]*State Key Laboratory of Fire Science, University of Science and Technology of China, Hefei, Anhui 230026, P.R. China. E-mail: yuanhu@ustc.edu.cn; Fax: +86-551-3601664; Tel: +86-551-3601664*
[b]*Department of Chemistry and Fire Retardant Research Facility, Marquette University, PO Box 1881, Milwaukee, WI, 53201, USA*
[c]*CAS Key Laboratory of Mechanical Behaviour and Design of Materials, Department of Modern Mechanics, University of Science and Technology of China, Hefei, Anhui 230026, P.R. China. E-mail: gongxl@ustc.edu.cn; Fax: +86-551-3600419; Tel: +86-551-3600419*

aspect of fire safety, was ambiguously attributed to the homogeneous heating caused by graphene,[22] the interaction between PS and graphene,[24] the jammed network of graphene which retarded transport of the decomposition products,[20] and the barrier effects of graphene which inhibited the mass transfer and shielded the underlying PS from the heat source, *etc.*[23] However, the mechanism is still not clear due to the lack of detailed research. Herein, the thermal degradation and combustion processes of Gs/PS composites are studied and compared so as to investigate the mechanism of the improved fire safe properties.

The dispersion of graphene in the polymer matrix is a key factor in the properties of GPNCs.[2–27] GPNCs are usually prepared by one of three techniques: (1) *in situ* polymerization, (2) solvent blending and (3) melt blending. The *in situ* polymerization and the solvent blending techniques usually result in good dispersion but require a lot of organic solvents, which is not convenient for industrial processing. Melt blending is very acceptable to the plastics industry but the dispersion is poor.[26–28] In order to prepare GPNCs with good dispersion by melt blending, a masterbatch-melt blending process was developed.[6] The masterbatch contains a high concentration of graphene, and is mixed with the polymer by melt blending (Fig. 2a). As compared with *in situ* polymerization and solvent blending, the use of organic solvents is significantly decreased; as compared with traditional melt blending, the dispersion and exfoliation of graphene is visibly improved.

Gs were prepared and incorporated into PS by masterbatch-melt blending. The dispersion of Gs in the PS matrix and the fire safety properties of Gs/PS composites, including thermal stability, heat release and CO yield, were studied. The mechanism for the improved dispersion and fire safety properties was discussed based on this study and previous works.

2. Experimental

2.1. Raw materials

Expandible graphite was supplied by Qingdao Tianhe Graphite Co., Ltd. (China). Sulfuric acid (H_2SO_4, 98%), potassium permanganate ($KMnO_4$), hydrazine hydrate (85% aq.), ammonia (25–28% aq.), hydrogen peroxide (H_2O_2, 30% aq.), hydrochloric acid (HCl, 37% aq., diluted to 5 wt% before use), zirconium oxychloride octahydrate ($ZrOCl_2 \cdot 8H_2O$), nickel chloride hexahydrate ($NiCl_2 \cdot 6H_2O$), and *N*,*N*-dimethylformamide (DMF) were obtained from Sinopharm Chemical Reagent Co., Ltd (China). PS (158 K) was obtained from BASF-YPC Co., Ltd (China). The graphite, H_2SO_4, $KMnO_4$ and a Teflon reactor (1000 mL) were cooled at 0 °C for 1 h before use.

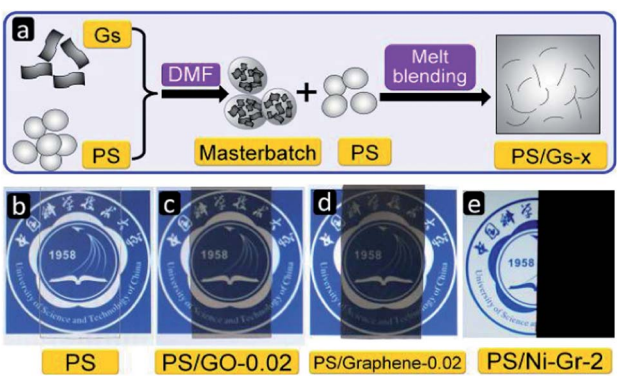

Fig. 2 (a) Preparation of the PS/Gs-*x* nanocomposites; (b–e) photographs of samples on the logo of the University of Science and Technology of China.

2.2. Preparation of Gs

GO was prepared by a pressurized oxidation in an autoclave consisting of a Teflon reactor and a stainless steel protector.[6] The cooled Teflon reactor was placed in the stainless steel protector. The cooled graphite (15 g), $KMnO_4$ (70 g) and H_2SO_4 (500 mL) were put into the reactor one after another *without* stirring. The closed autoclave was put in a refrigerator (0 °C) for 1.5 h and then heated at 100 °C in an oven for 1.5 h. The autoclave must be *tightly sealed* before putting into the oven. The obtained viscous mud was diluted in water with stirring. H_2O_2 was added to the mixture until it turned yellow. The suspension was left to stand until the products were fully precipitated. The deposit was collected, washed with the diluted HCl and deionized water. The obtained humid GO was dispersed in deionized water (totally 6.7 mg/mL) with 2 h of ultrasonication and strong mechanical stirring to reduce the particle sizes.[6]

Graphene was prepared from GO by the ammonia–hydrazine reduction.[6] Ammonia (4 mL per 1 g GO) was added to the GO, and hydrazine (3 mL per 1 g GO) was added 1 h later. After 2 h of ultrasonication and stirring, the flask was heated at 100 °C for 24 h with reflux and mechanical stirring. The obtained black product was filtered with a Buchner funnel and washed with deionized water.

Zr–Gr and Ni–Gr were prepared by the hydrothermal method (Fig. 1). $ZrOCl_2 \cdot 8H_2O$ and $NiCl_2 \cdot 6H_2O$ (0.05 mol per 1 g GO), respectively, were dissolved in deionized water, mixed with GO and stirred for 2 h. The blend of $ZrOCl_2 \cdot 8H_2O$/GO was placed into an autoclave reactor and heated at 200 °C for 6 h. Ammonia was added to the $NiCl_2 \cdot 6H_2O$/GO blend with stirring until the pH reached 10. The blend was reacted at 200 °C for 6 h under hydrothermal conditions. The products were filtered and washed with deionized water.

Most of the Gs were kept humid, and a small portion was dried at 80 °C in an oven for 24 h for characterization.

2.3. Preparation of PS/Gs-*x*

The Gs/PS composites were prepared by masterbatch-melt blending (Fig. 2a).[6] Samples were titled PS/Gs-*x*, where "*x*" is the mass ratio of Gs (0.02%, 0.1% and 2%).

The humid Gs were washed with DMF four times to remove water. Gs were dispersed (120 mL DMF per 1 g Gs) in DMF in a 3-necked round-bottom flask with 1 h of ultrasonication and strong mechanical stirring. PS (9 g PS per 1 g Gs) was marinated in DMF (4 mL DMF per 1 g PS) for 0.5 h, and then, the mixture was added to the Gs/DMF blend. After 2 h of ultrasonication and strong mechanical stirring, the obtained black slurry was dried in an oven at 120 °C for 12 h, cut into small platelets and further dried at 130 °C in a vacuum oven for 6 h. The mass ratio of Gs was 10% in the masterbatch.

Certain amounts of the masterbatch were mixed with PS by melt blending at 180 ± 3 °C. PS/GO-*x* and PS/graphene-*x* were prepared on a twin-roller Banbury mixer (SU-70ML, Changzhou Suyuan Rubber and Plastic Science and Technology Co., Ltd, 180 ± 3 °C, roller speed of 50 rpm, 8 minutes mixing). PS/Zr–Gr-*x* and PS/Ni–Gr-*x* were prepared on a twin-screw extruder (LSSJ-20, Shanghai Kechuang Rubber and Plastic Instruments Co., Ltd, screw speed of 60 rpm, extruded three times). The samples were hot-pressed into sheets at 190 °C (1.0 mm thick).

2.4. Characterization

Atomic force microscope (AFM) was performed using a Veeco DI Multimode V scanning probe microscope. Samples were dispersed in water with 10 minutes of ultrasonication and dip-coated onto freshly cleaved mica surfaces before observation.

Transmission electron microscopy (TEM, JEM-2011, Japan Electron Optics Laboratory) was employed to investigate the morphology of Gs and the dispersion of Gs in PS. Gs were dispersed in water with 10 min of ultrasonication and dripped onto copper grids; PS/Gs-2 samples were microtomed to ultra-thin sections using a Du Pont MT-6000 Ultratome and transferred onto copper grid for observation.

X-ray diffraction (XRD) were performed with a Rigaku D-Max-Ra rotating anode X-ray diffractometer equipped with a Cu-Kα tube and a Ni filter ($\lambda = 0.1542$ nm).

X-ray photoelectron spectroscopy (XPS) was performed with a VG ESCALB MK-II electron spectrometer. The excitation source was an Al Kα line at 1486.6 eV.

Fourier-transform infrared (FTIR) spectra were obtained on a Nicolet 6700 FTIR instrument. The dried Gs was mixed with KBr powder and pressed into tablets.

Photographs of PS and PS/Gs-*x* were obtained using a Sony DCR-SR65 digital camera.

Thermal degradation was investigated by a TA Q5000 thermo-analyzer. Samples were heated at a linear rate of 20 °C min^{-1} from room temperature to 700 °C in a nitrogen atmosphere.

The combustion properties of PS/Gs-*x* were investigated using a Stanton Redcroft cone calorimeter according to ISO 5660-1 standard. Every sample was heated at a heat flux of 35 kW m^{-2}.

3. Results and discussion

3.1. Characterization of Gs

Detailed discussions of GO and graphene are available in our previous work.[6]

The morphology of GO (Fig. 3a) and graphene (Fig. 3b) was investigated by AFM. The thickness of GO is 1.1 nm, and the width is 1–2 μm. The thickness of graphene is 0.4–0.5 nm, and the width is 0.3–0.7 μm. The layers of GO (Fig. 3c) and graphene (Fig. 3d) are clean, while Zr–Gr (Fig. 3e) and Ni–Gr (Fig. 3f) have many small and dark particles attached. The graphene in Zr–Gr and Ni–Gr was so thin that some of the graphene edges are nearly invisible (Fig. 3e and f). The dark particles in Zr–Gr and Ni–Gr are ZrO_2 and β-$Ni(OH)_2$, respectively.

XRD was employed to investigate the structure of the loaded metal compounds. The indexing of the XRD patterns is shown in Fig. 4a. GO has a typical diffraction peak at $2\theta = 10.7°$, and graphene has a very weak diffraction at $2\theta = 20$–$30°$.[6] The XRD

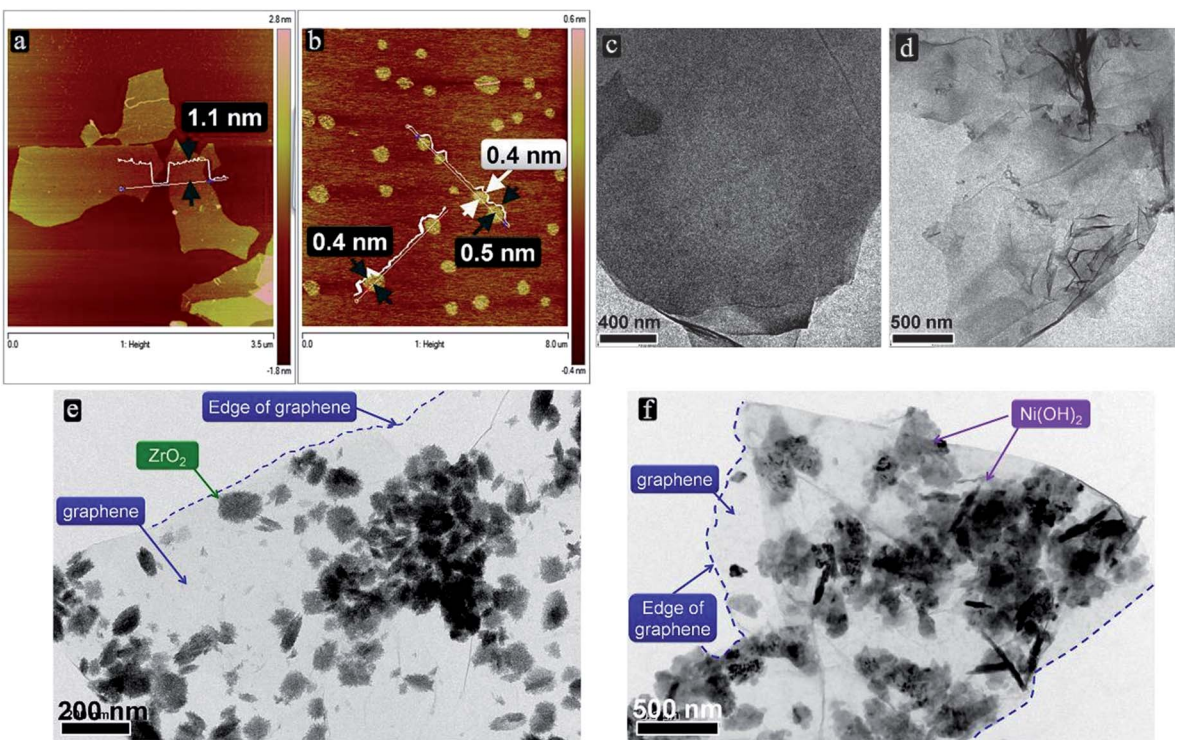

Fig. 3 Morphology of Gs: (a) AFM profile of GO; (b) AFM profile of graphene; (c) TEM profile of GO; (d) TEM profile of graphene; (e) TEM profile of Zr–Gr; and (f) TEM profile of Ni–Gr.

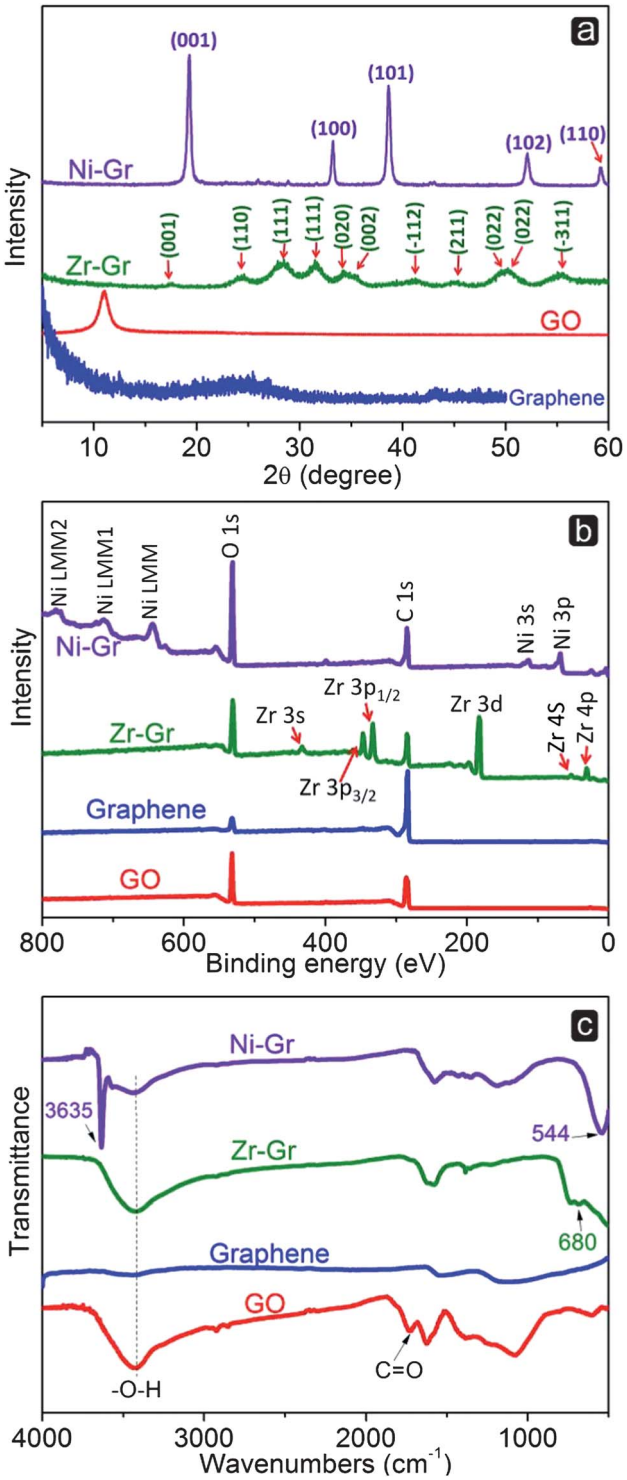

Fig. 4 Characterization of Gs : (a) XRD; (b) XPS; and (c) FTIR profiles.

patterns of Ni–Gr and Zr–Gr present the typical diffraction of β-$Ni(OH)_2$ and the monoclinic phase of ZrO_2, respectively.[29–31]

The elemental composition of Gs was investigated by XPS, as shown in Fig. 4b and Table 1. The XPS peaks of Zr–Gr and Ni–Gr agree well with those of ZrO_2[32] and β-$Ni(OH)_2$ in earlier work.[33] The C/O atomic ratio of GO is 2.12 and it is 9.00 in graphene, indicating a high degree of reduction. The C/O atomic ratio of Zr–Gr is 1.17. There is 40% oxygen and 13% zirconium in

Table 1 The elemental component of Gs

Gs	Carbon	Oxygen	Metal
GO	68%	32%	—
Graphene	90%	10%	—
Zr–Gr	47%	40%	13% Zr
Ni–Gr	40%	41%	19% Ni

Zr–Gr (Table 1), so 26% of the oxygen is from ZrO_2, and the rest 14% is from the graphene. Therefore, the true C/O atomic ratio of the graphene in Zr–Gr is 3.36 (47% : 14%). It is higher than that of GO (2.12) because it was partially reduced under hydrothermal conditions.[34,35] The true C/O ratio of Ni–Gr is 13.33, which is higher than GO, graphene and Zr–Gr due to the combination of the hydrothermal conditions and the use of ammonia.[36,37]

The functional groups in Gs were investigated by FTIR (Fig. 4c). In the spectrum of GO, there are several typical absorption peaks: C–O (1000–1300 cm^{-1}), C–OH (1382 cm^{-1}), water (1623 cm^{-1}), C=O (1725 cm^{-1}), alkyl groups (2800–2950 cm^{-1}) and hydroxyl (3428 cm^{-1}).[38–41] In the spectrum of graphene, all of the bands are very weak, and a peak at 1562 cm^{-1}, which is assumed to be the C=C in graphitic domains, becomes notable, suggesting a high degree of reduction. The weak bands of C–O (1000–1300 cm^{-1}) and hydroxyl (~3400 cm^{-1}) imply very few oxygen-containing groups in the graphene. The peak of water (1623 cm^{-1}) disappears due to the hydrophobic character of graphene. In the spectra of Zr–Gr, the bands at 500–850 cm^{-1} are assigned to Zr–O bonds, and the peak at about 680 cm^{-1} is typical of ZrO_2.[42–44] In the spectra of Ni–Gr, the peak at 3635 cm^{-1} is due to the –OH in β-$Ni(OH)_2$, and the band around 544 cm^{-1} is assigned as the angular deformation in plane of the hydroxyl in both β-$Ni(OH)_2$ and water.[29,33]

Based on the above information, it is clear that ZrO_2 and β-$Ni(OH)_2$ have been successfully loaded onto graphene.

3.2. The dispersion of Gs

Fig. 2b–e shows the photographs of PS/Gs-*x*. The film of neat PS is transparent (Fig. 2b). With 0.02% Gs, the film turns semi-transparent with uniform brown colour (Fig. 2c and d), indicating good dispersion at the macroscopic scale. The film of PS/Ni–Gr-2 is black and not transparent at all (Fig. 2e).

Fig. 5 presents the TEM observation of the PS/Gs-2 ultrathin sections. The dark lines in Fig. 5a are the side views of GO while the thin lines are the exfoliated GO layers, and the thick lines are the un-exfoliated or folded layers. Some of the layers are folded due to extrusion and tearing during melt blending. Most of the graphene nanolayers in Fig. 5b are well dispersed and highly exfoliated. The high resolution observation of Area 1 shows the transition state from stacking to exfoliation, implying that the graphene is exfoliated by the shearing of the viscous melt of PS. The thin lines in Fig. 5c and d are the side views of the graphene in Zr–Gr and Ni–Gr, and the thick and dark speckles are assumed to be ZrO_2 and β-$Ni(OH)_2$, respectively. Most of the metal compounds are no longer attached to the graphene surface, probably due to ultrasonication, stirring and shearing during the preparation of the masterbatch and the melt-compounding.

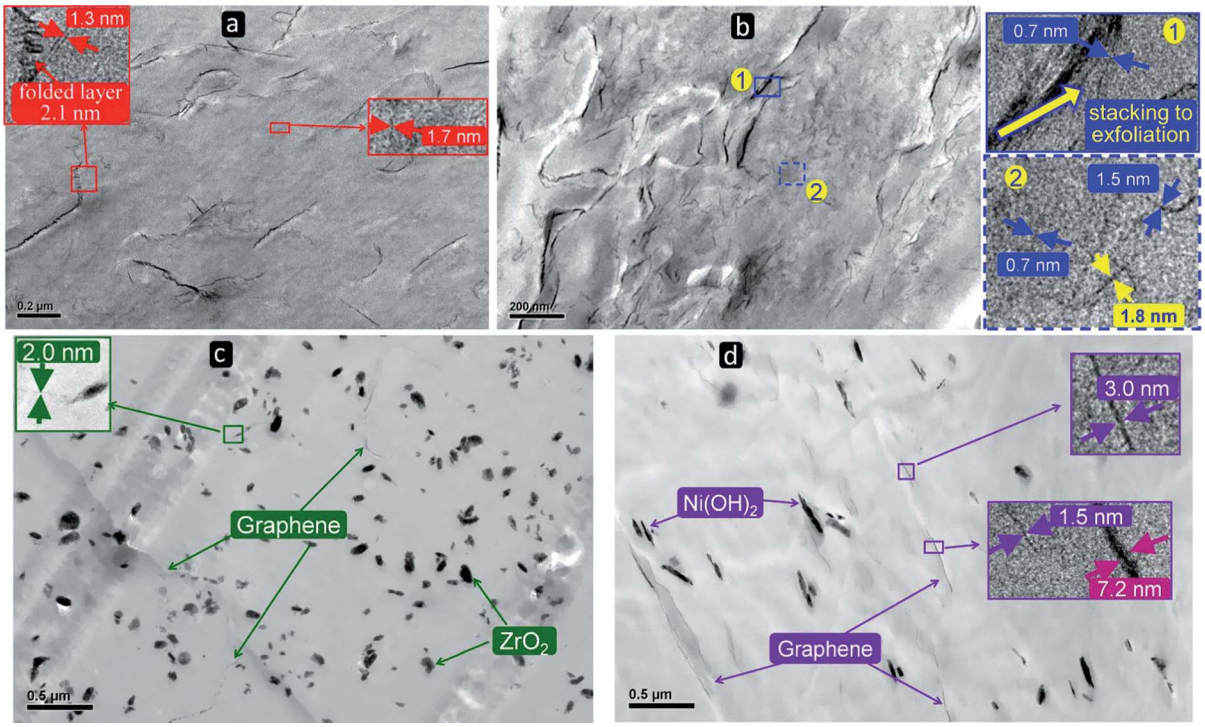

Fig. 5 TEM photographs of the PS/Gs-2 ultrathin sections. The inset images are high resolution observations. (a) PS/GO-2; (b) PS/Graphene-2; (c) PS/Zr–Gr-2; the thin lines are the side views of graphene and the thick speckles are assumed to ZrO_2 particles; and (d) PS/Ni–Gr-2, the thin lines are graphene layers and the thick lines are β-$Ni(OH)_2$ layers.

As shown in Fig. 5a and b, GO and graphene are exfoliated to thin layers, some of which are not even visible in the low resolution profiles. Most of the nanolayers are less than 2 nm thick, and some cases the layers are only 0.7 nm thick (Fig. 5b), indicating bi-layer or even monolayer of graphene. The small thickness indicates a high degree of exfoliation. Qi *et al.* prepared graphene/PS nanocomposites by solvent blending. The graphene was well dispersed but poorly exfoliated: the thickness was more than 20 nm.[21] Kim *et al.* prepared GO/polyurethane (PU) and graphene/PU nanocomposites, by melt blending, solvent blending and *in situ* polymerization,[45] and the thickness of the GO or graphene was larger than 5 nm. The thickness of graphene nanolayers in GPNCs is almost always more than 5 nm, whether prepared by melt blending, solvent blending, or *in situ* polymerization,[8,21,22,45–59] so the dispersion and exfoliation of the Gs in Fig. 5 are among the best ever seen.

The good dispersion and exfoliation can be attributed to: (1) the PS in the masterbatch prevents the Gs from stacking during the evaporation and melt-compounding; and (2) the high matrix viscosity in the melt-compounding step combines tearing and exfoliating graphene.[45] This *prevention* effect is not available in traditional melt blending, and the *high matrix viscosity* is not available in traditional solvent blending and *in situ* polymerization. Masterbatch-melt blending combines the advantages from the three traditional blending methods, achieving good dispersion and exfoliation, and is compatible with current industrial processing techniques (melt millers and twin-screw extruders).

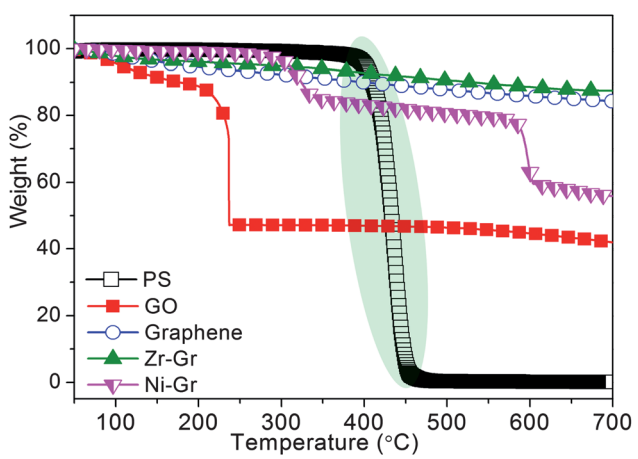

Fig. 6 TGA curves of Gs and PS.

3.3. Fire safety properties

Thermogravimetric analysis (TGA) was employed to investigate the thermal degradation of Gs, PS and PS/Gs-*x*. The TGA curves of GO, graphene and neat PS are shown in Fig. 6. GO starts losing weight below 100 °C due to desorption of the adsorbed water. GO has a significant loss at 210–240 °C due to decomposition of oxygen-containing groups such as epoxy, hydroxyl and carboxyl.[6] In the case of graphene and Zr–Gr, steady loss is observed up to 700 °C. The TGA curves of Ni–Gr presents two steps of mass loss at 280–360 °C (14%) and 570–620 °C (19.5%). The thermal degradation of PS occurs in the range of 390–470 °C.

Layered nanofillers usually increase the thermal stability of a polymer due to the physical barrier effect which retards the diffusion of degradation products, gases and heat.[11–14] In the temperature range of 390–470 °C where PS is degraded, GO is largely decomposed (47% residue) while graphene (89% residue)

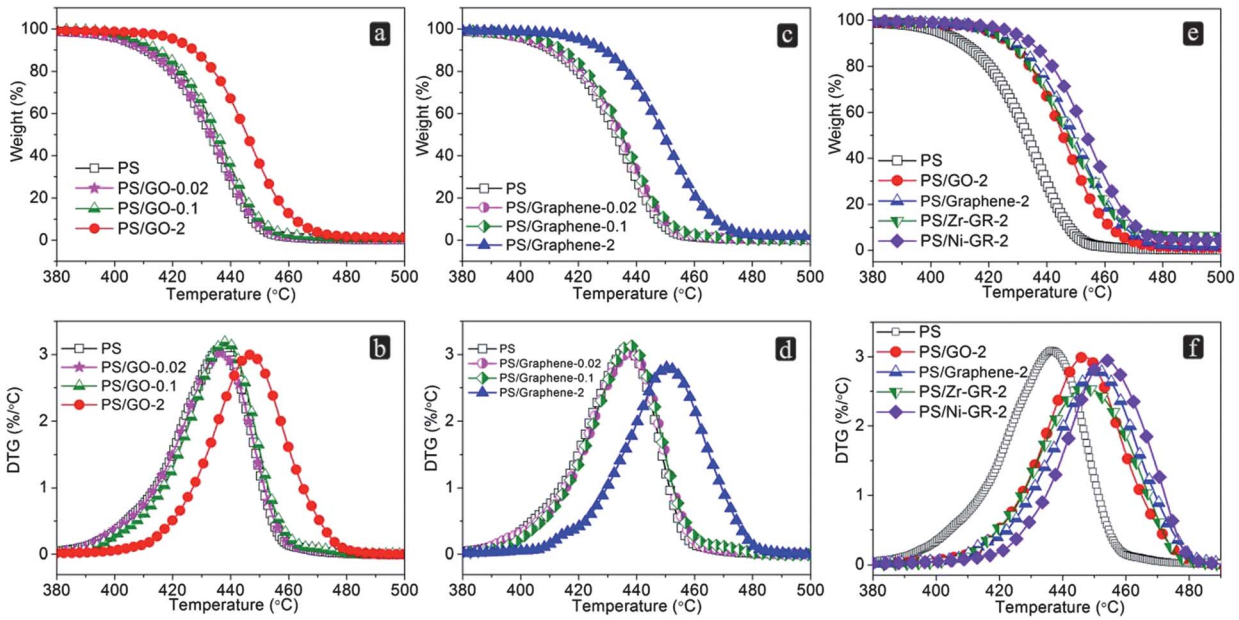

Fig. 7 TGA and DTG curves of PS/GO-*x* (a and b) and PS/graphene-*x* (c and d), and the comparison between PS/Gs-2 composites (e and f).

is only slightly decomposed, so graphene must present better physical barrier effects than GO, which may increase the thermal stability in GPNCs. However, the high thermal conductivity of graphene, which speeds-up the diffusion of heat in the PS matrix, may decrease the thermal degradation temperature (T_{-d}) of GPNCs. GO has lower thermal conductivity than graphene due to its structure defects.[60–63] Therefore, comparison between PS/GO-*x* and PS/graphene-*x* will offer evidence to clarify which, the physical barrier effect or the high thermal conductivity, is more important in influencing the thermal stability of GPNCs.

The TGA curves of the PS/Gs-*x* composites are shown in Fig. 7. The T_{-d} of PS/Gs-*x* increases compared with neat PS; the high thermal conductivity of graphene, which opposes an increase of T_{-d}, has little effect on the T_{-d} of PS. The temperature of maximum degradation in the differential thermogravimetric (DTG) curve (T_{-max}) of PS is 436 °C. In PS/Gs-0.02 and PS/Gs-0.1, the increase of T_{-d} is very small; in PS/Gs-2, the T_{-d} is increased by more than 10 °C (Fig. 7b, d and f). The TGA and DTG curves of PS/Gs-2 are shown in Fig. 7e and f. PS/Zr–Gr-2 has the smallest DTG peak, and PS/Ni–Gr-2 has the highest T_{-max} (454 °C). PS/graphene-2 has a higher T_{-d} than PS/GO-2 although graphene has higher thermal conductivity than GO. Therefore, the high thermal conductivity must not be a decisive factor in the T_{-d}, and it should be attributed to the physical barrier effect which retards the diffusion and release of the degradation products.[20,23]

In our earlier works, the T_{-d} of GPNCs was sometimes decreased due to the high thermal conductivity.[6,64] However, the T_{-d} is always increased in this work. So there must be other factors, besides the physical barrier effect and the high thermal conductivity, that influence the thermal stability of GPNCs. The interaction between graphene and the polymer is one strong possibility.[24] The increases of the T_{-max} in our recent works are collected in Fig. 8. There is a strong π–π interaction between PS and Gs, and the T_{-max} is always increased; there is strong hydrogen bonding between poly(vinyl alcohol) (PVA) and GO, and the T_{-max} is always increased;[64] there is some, but not much, hydrogen bonding between PVA and graphene, and the T_{-max} is decreased with a small addition and increased with a large addition of graphene;[64] there is no strong interaction between PLA and graphene, and the T_{-max} of graphene/PLA nanocomposites is always decreased.[6] Thus, it is reasonable that the interaction between Gs and the polymer plays an important role in the improved thermal stability. This study and the research of graphene/PVA and GO/PVA nanocomposites confirm the importance of the physical barrier effect of graphene (or Gs).[64] Therefore, the physical barrier effect of graphene and the interaction between graphene and polymers are two key factors to improve the thermal stability of GPNCs.

Fig. 9 shows the heat release rate (HRR), total release rate (THR) and CO concentration collected from the cone calorimeter. The ignition time of PS/Gs-*x* was not increased at all, probably due to the high thermal conductivity of Gs. No improvement is obtained in PS/Gs-0.1 (Fig. 9a), while the PS/Gs-2 composites have visibly smaller PHRR than does the virgin PS.

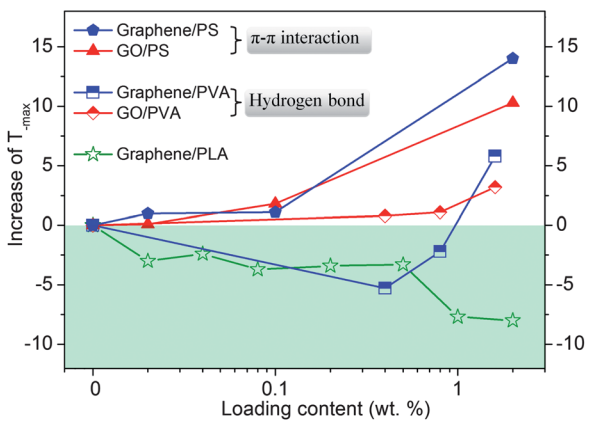

Fig. 8 Increases of the T_{-max} in this and our earlier works.

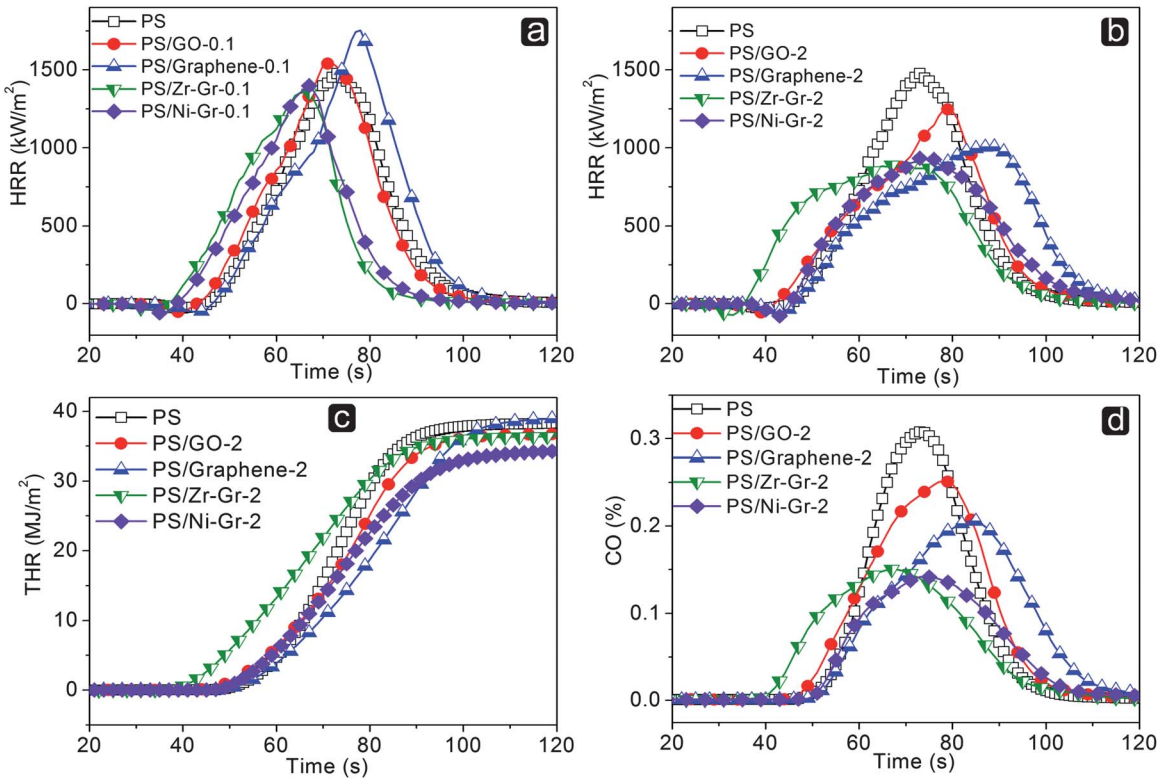

Fig. 9 Cone data: (a and b) HRR curves; (c) THR curves; and (d) CO production.

The largest reduction of PHRR was obtained in PS/Zr–Gr-2 (40%) and PS/GO-2 exhibits the smallest reduction of PHRR, probably due to its poor physical barrier effect caused by the structural defects and poor thermal stability of GO (Fig. 6). The THR of PS is 38.2 MJ m^{-2}, and the maximum decrease is 9% (PS/Ni–Gr-2) which is within the margin of error, indicating that Gs have little effect on the THR. Fig. 9d shows the CO concentration curves of PS/Gs-2. PS/Zr–Gr-2 (51%) and PS/Ni–Gr-2 (54%) cause an obvious decrease while GO (19%) and graphene (33%) cause less of a decrease. TEM (Fig. 5) shows PS/Zr–Gr-2 and PS/Ni–Gr-2 have fewer graphene layers than PS/GO-2 and PS/graphene-2, but they perform better at decreasing the PHRR and CO concentration, presumably due to the synergistic effect of the metal compounds.[15–17,65] Therefore, the physical barrier effect of Gs and the synergistic effect of the metal compounds should be the main reasons for the reduced PHRR and CO concentration. However, the effect of the interface interaction on the combustion properties is still not clear.

4. Conclusions

GO was prepared by pressurized oxidation, graphene by the ammonia–hydrazine reduction, and Zr–Gr and Ni–Gr by hydrothermal synthesis. GO, graphene, Zr–Gr and Ni–Gr are all well dispersed and exfoliated in PS by masterbatch-melt blending. The fire safety properties of the PS/Gs-*x* composites were improved, including increased thermal degradation temperature (18 °C, PS/Ni–Gr-2), and decreased PHRR (40%, PS/Zr–Gr-2) and CO concentration (54%, PS/Ni–Gr-2). The physical barrier effect of Gs, the interaction between Gs and the polymer, and the synergism of the metal compounds are the main causes of the improvements. The combination of graphene and metal-compounds may contribute a promising strategy to the improvement of the fire safety of polymers.

Acknowledgements

This work was supported by the National Basic Research Program of China (973 Program, no. 2012CB719701), National Natural Science Foundation of China (Grant No. 11125210) and the joint fund of National Natural Science Foundation of China and Civil Aviation Administration of China (no. 61079015).

References

1 K. P. Loh, Q. L. Bao, P. K. Ang and J. X. Yang, *J. Mater. Chem.*, 2010, **20**, 2277–2289.
2 X. Huang, X. Y. Qi, F. Boey and H. Zhang, *Chem. Soc. Rev.*, 2012, **41**, 666–686.
3 V. Singh, D. Joung, L. Zhai, S. Das, S. I. Khondaker and S. Seal, *Prog. Mater. Sci.*, 2011, **56**, 1178–1271.
4 Y. W. Zhu, S. Murali, W. W. Cai, X. S. Li, J. W. Suk, J. R. Potts and R. S. Ruoff, *Adv. Mater.*, 2010, **22**, 3906–3924.
5 M. S. Lundstrom, *Nat. Mater.*, 2011, **10**, 566–567.
6 C. L. Bao, L. Song, W. Y. Xing, B. H. Yuan, C. A. Wilkie, J. L. Huang, Y. Q. Guo and Y. Hu, *J. Mater. Chem.*, 2012, **22**, 6088–6096.
7 X. Wang, L. Song, H. Y. Yang, W. Y. Xing, H. D. Lu and Y. Hu, *J. Mater. Chem.*, 2012, **22**, 3426–3431.
8 Y. Q. Guo, C. L. Bao, L. Song, B. H. Yuan and Y. Hu, *Ind. Eng. Chem. Res.*, 2011, **50**, 7772–7783.
9 Y. Qu and Y. S. Tong, *Safety*, 2008, **29**, 6–8.
10 X. W. Zhao, *Fire Tech. Prod. Inform.*, 2009, **2009**, 5–9.
11 P. Kiliaris and C. D. Papaspyrides, *Prog. Polym. Sci.*, 2010, **35**, 902–958.
12 S. Bourbigot and S. Duquesne, *J. Mater. Chem.*, 2007, **17**, 2283–2300.

13 P. Ding, W. Chen and B. J. Qu, *Prog. Nat. Sci.*, 2006, **16**, 573–579.
14 A. Leswzynska, J. Njuguna, K. Pielichowski and J. R. Banerjee, *Thermochim. Acta*, 2007, **454**, 1–22.
15 M. Lewin and M. Endo, *Polym. Adv. Technol.*, 2003, **14**, 3–11.
16 D. D. Yang, Y. Hu, L. Song, S. B. Nie, S. Q. He and Y. B. Cai, *Polym. Degrad. Stab.*, 2008, **93**, 2014–2018.
17 A. Rodolfo and L. H. I. Mei, *J. Appl. Polym. Sci.*, 2010, **118**, 2613–2623.
18 D. J. Carastan and N. R. Demarquette, *Int. Mater. Rev.*, 2007, **52**, 345–380.
19 J. T. Yang, H. Fan, Z. Y. Bu and B. G. Li, *Polym. Eng. Sci.*, 2009, **49**, 1937–1944.
20 V. H. Pham, T. V. Cuong, T. T. Dang, S. H. Hur, B. S. Kong, E. J. Kim, E. W. Shin and J. S. Chung, *J. Mater. Chem.*, 2011, **21**, 11312–11316.
21 X. Y. Qi, D. Yan, Z. G. Jiang, Y. K. Cao, Z. Z. Yu, F. Yavari and N. Koratkar, *ACS Appl. Mater. Interfaces*, 2011, **3**, 3130–3133.
22 H. T. Hu, X. B. Wang, J. C. Wang, L. Wan, F. M. Liu, H. Zheng, R. Chen and C. H. Xu, *Chem. Phys. Lett.*, 2010, **484**, 247–253.
23 A. S. Patole, S. P. Patole, H. Kang, J. B. Yoo, T. H. Kim and J. H. Ahn, *J. Colloid Interface Sci.*, 2010, **350**, 530–537.
24 M. Z. Kassaee, E. Motamedi and M. Majdi, *Chem. Eng. J.*, 2011, **172**, 540–549.
25 D. Y. Cai and M. Song, *J. Mater. Chem.*, 2010, **20**, 7906–7915.
26 J. R. Potts, D. R. Dreyer, C. W. Bielawski and R. S. Ruoff, *Polymer*, 2011, **52**, 5–25.
27 H. Kim, A. A. Abdala and C. W. Macosko, *Macromolecules*, 2010, **43**, 6515–6530.
28 R. Verdejo, M. M. Bernal, L. J. Romasanta and M. A. Lopez-Manchado, *J. Mater. Chem.*, 2011, **21**, 3301–3310.
29 M. Freitas, *J. Power Sources*, 2001, **93**, 163–173.
30 Y. Zhang, F. G. Xu, Y. J. Sun, Y. Shi, Z. W. Wen and Z. Li, *J. Mater. Chem.*, 2011, **21**, 16949–16954.
31 Y. Wang, D. X. Cao, G. L. Wang, S. S. Wang, J. Y. Wen and J. L. Yin, *Electrochim. Acta*, 2011, **56**, 8285–8290.
32 S. Tsunekawa, K. Asami, S. Ito, M. Yashima and T. Sugimoto, *Appl. Surf. Sci.*, 2005, **252**, 1651–1656.
33 B. J. Li, H. Q. Cao, J. Shao, H. Zheng, Y. X. Lu, J. F. Yin and M. Z. Qu, *Chem. Commun.*, 2011, **47**, 3159–3161.
34 Y. Zhou, Q. L. Bao, L. A. L. Tang, Y. L. Zhong and K. P. Loh, *Chem. Mater.*, 2009, **21**, 2950–2956.
35 Y. X. Xu, K. X. Sheng, C. Li and G. Q. Shi, *ACS Nano*, 2010, **4**, 4324–4330.
36 D. H. Long, W. Li, L. C. Ling, J. Miyawaki, I. Mochida and S. H. Yoon, *Langmuir*, 2010, **26**, 16096–16102.
37 I. Janowska, K. Chizari, O. Ersen, S. Zafeiratos, D. Soubane, V. Da Costa, V. Speisser, C. Boeglin, M. Houlle, D. Begin, D. Plee, M. J. Ledoux and C. Pham-Huu, *Nano Res.*, 2010, **3**, 126–137.
38 H. L. Guo, X. F. Wang, Q. Y. Qian, F. B. Wang and X. H. Xia, *ACS Nano*, 2009, **3**, 2653–2659.
39 A. Bagri, C. Mattevi, M. Acik, Y. J. Chabal, M. Chhowalla and V. B. Shenoy, *Nat. Chem.*, 2010, **2**, 581–587.
40 J. F. Ou, J. Q. Wang, S. Liu, B. Mu, J. F. Ren, H. G. Wang and S. R. Yang, *Langmuir*, 2010, **26**, 15830–15836.
41 Z. P. Li, Y. J. Mi, X. H. Liu, S. Liu, S. R. Yang and J. Q. Wang, *J. Mater. Chem.*, 2011, **21**, 14706–14711.
42 T. Otsuka and Y. Chujo, *Polym. J.*, 2010, **42**, 58–65.
43 L. Koltunski and R. A. B. Devine, *Appl. Phys. Lett.*, 2001, **79**, 320–322.
44 G. Gonzalez, C. Albano, V. Herman, I. Boyer, A. Monsalve and J. A. Brito, *Mater. Charact.*, 2012, **64**, 96–106.
45 H. Kim, Y. Miura and C. W. Macosko, *Chem. Mater.*, 2010, **22**, 3441–3450.
46 G. Vleminckx, S. Bose, J. Leys, J. Vermant, M. Wubbenhorst, A. A. Abdala, C. Macosko and P. Moldenaers, *ACS Appl. Mater. Interfaces*, 2011, **3**, 3172–3180.
47 J. T. Yang, M. J. Wu, F. Chen, Z. D. Fei and M. Q. Zhong, *J. Supercrit. Fluids*, 2011, **56**, 201–207.
48 A. V. Raghu, Y. R. Lee, H. M. Jeong and C. M. Shin, *Macromol. Chem. Phys.*, 2008, **209**, 2487–2493.
49 D. A. Nguyen, Y. R. Lee, A. V. Raghu, H. M. Jeong, C. M. Shin and B. K. Kim, *Polym. Int.*, 2009, **58**, 412–417.
50 S. Ansari and E. P. Giannelis, *J. Polym. Sci., Part B: Polym. Phys.*, 2009, **47**, 888–897.
51 H. Kim and C. W. Macosko, *Polymer*, 2009, **50**, 3797–3809.
52 R. Wissert, P. Steurer, S. Schopp, R. Thomann and R. Mulhaupt, *Macromol. Mater. Eng.*, 2010, **295**, 1107–1115.
53 H. B. Zhang, W. G. Zheng, Q. Yan, Y. Yang, J. W. Wang, Z. H. Lu, G. Y. Ji and Z. Z. Yu, *Polymer*, 2010, **51**, 1191–1196.
54 R. C. Feng, G. H. Guan, W. Zhou, C. C. Li, D. Zhang and Y. N. Xiao, *J. Mater. Chem.*, 2011, **21**, 3931–3939.
55 H. Kim, S. Kobayashi, M. A. AbdurRahim, M. L. J. Zhang, A. Khusainova, M. A. Hillmyer, A. A. Abdala and C. W. Macosko, *Polymer*, 2011, **52**, 1837–1846.
56 P. G. Ren, D. X. Yan, T. Chen, B. Q. Zeng and Z. M. Li, *J. Appl. Polym. Sci.*, 2011, **121**, 3167–3174.
57 J. R. Potts, S. H. Lee, T. M. Alam, J. An, M. D. Stoller, R. D. Piner and R. S. Ruoff, *Carbon*, 2011, **49**, 2615–2623.
58 I. Zaman, T. T. Phan, H. C. Kuan, Q. S. Meng, L. T. B. La, L. Luong, O. Youssf and J. Ma, *Polymer*, 2011, **52**, 1603–1611.
59 B. Shen, W. T. Zhai, C. Chen, D. D. Lu, J. Wang and W. G. Zheng, *ACS Appl. Mater. Interfaces*, 2011, **3**, 3103–3109.
60 J. N. Hu, X. L. Ruan and Y. P. Chen, *Nano Lett.*, 2009, **9**, 2730–2735.
61 D. L. Nika, E. P. Pokatilov, A. S. Askerov and A. A. Balandin, *Phys. Rev. B: Condens. Matter Mater. Phys.*, 2009, **79**, 155413.
62 F. Hao, D. N. Fang and Z. P. Xu, *Appl. Phys. Lett.*, 2011, **99**(4), 041901.
63 J. Haskins, A. Kinaci, C. Sevik, H. Sevincli, G. Cuniberti and T. Cagin, *ACS Nano*, 2011, **5**, 3779–3787.
64 C. L. Bao, Y. Q. Guo, L. Song and Y. Hu, *J. Mater. Chem.*, 2011, **21**, 13942–13950.
65 H. D. Lu, C. A. Wilkie, M. Ding and L. Song, *Polym. Degrad. Stab.*, 2011, **96**, 885–891.

